EAI Endorsed Transactions
on Pervasive Health and Technology
Research Article EAI.EU

CT-Based Morphometric Analysis of Proximal Humerus Fractures: A Quantitative Framework

Thy Gia Anh Le[1], Thi Cao[2*], Thuy Hoang Vinh Le[1], Khang Kha Bao Cao[2]

[1]Hospital for Traumatology and Orthopaedics in Ho Chi Minh City
[2]University of Medicine and Pharmacy at Ho Chi Minh City

Abstract

INTRODUCTION: Radiographs may underestimate displacement in proximal humeral fractures (PHFs).
OBJECTIVES: To develop a CT framework integrating fracture morphology, bone quality, and imaging features associated with humeral-head ischemic risk.
METHODS: Eighty PHF CT scans were retrospectively assessed using standardized multiplanar reconstruction. Tuberosity displacement, neck–shaft angle, calcar length, medial hinge displacement, deltoid tuberosity index (DTI), Hounsfield units (HU), and Hertel criteria were evaluated.
RESULTS: The mean age was 53.7 ± 16.2 years; 67.5% were women and 61.3% had two-part fractures. Mean DTI was 1.75 ± 0.32 and HU 125.1 ± 6.3; 20% had DTI<1.44. In surgical-neck fractures, calcar length was 6.58 ± 2.47 mm, hinge displacement 1.66 ± 2.17 mm, and 81.6% met ≥2 predefined Hertel-related ischemic-risk features. Complexity was associated with direct trauma ($p<0.01$), but not age, sex, low DTI status, or HU.
CONCLUSION: CT morphometry quantifies PHF morphology and bone quality and may support computer-aided tools.

Keywords: proximal humerus fracture, computed tomography, morphometry, Hertel criteria, deltoid tuberosity index, Hounsfield unit; bone quality

Received on 19 October 2025, accepted on 06 October 2026, published on 02 November 2026

Copyright © 2026 Thy Gia Anh Le *et al.*, licensed to EAI. This is an open access article distributed under the terms of the CC BY-NC-SA 4.0, which permits copying, redistributing, remixing, transformation, and building upon the material in any medium so long as the original work is properly cited.

doi: 10.4108/eetpht.11.10651

*Corresponding author. Email: caothibacsi@ump.edu.vn

1. Introduction

Proximal humeral fractures (PHFs) account for approximately 4–5% of all fractures and occur predominantly in older adults, particularly women with osteoporosis [1,2]. In younger patients, PHFs are more commonly associated with high-energy trauma, whereas low-energy falls predominate in the elderly. Court-Brown et al. [3] reported that most PHFs in patients aged ≥65 years resulted from low-energy falls.

Accurate characterization of fracture morphology is important for classification and treatment planning. The Neer

and AO/OTA systems are widely used to describe fracture patterns, while Hertel criteria incorporate specific morphological features associated with humeral-head ischemic risk [4]. However, conventional radiographs may incompletely characterize fragment displacement, articular involvement, and complex fracture configurations. Computed tomography (CT), particularly multiplanar reconstruction (MPR) and three-dimensional (3D) reconstruction, provides more detailed visualization of fracture morphology and may improve fracture characterization and classification [5–7].

Beyond conventional classification, quantitative CT assessment can provide objective measurements of fracture morphology and bone quality. Parameters such as tuberosity displacement, neck–shaft angle, medial calcar length, medial hinge displacement, and head-split displacement may characterize fracture configuration and features associated with humeral-head ischemic risk. In addition, CT-derived indices such as the deltoid tuberosity index (DTI) and Hounsfield units (HU) may provide information on local bone quality. Integrating these measurements within a standardized MPR-based assessment may therefore provide a more structured description of PHFs than categorical classification alone.

Despite increasing use of CT for PHF assessment, quantitative CT-based morphometric data remain limited, particularly in Vietnamese populations. Moreover, fracture morphology, ischemic-risk features, and CT-based bone-quality indices are often evaluated separately rather than within a unified quantitative framework. Therefore, this study aimed to characterize the CT-based morphometric features of PHFs and to develop a quantitative framework integrating fracture morphology, bone-quality indices, and imaging features associated with humeral-head ischemic risk.

2. Materials and methods

2.1 Study Design and Dataset

This retrospective descriptive study analyzed non-contrast computed tomography (CT) scans of patients with proximal humeral fractures (PHFs) performed at the Department of Radiology, Hospital for Traumatology and Orthopaedics, Ho Chi Minh City, between January 2024 and April 2025. All CT datasets were retrieved from the Picture Archiving and Communication System (PACS) and de-identified before analysis.

For the quantitative morphometric analysis, the CT-derived dataset was formally represented as:

$$D = \{x_i\}_(i = 1)\^N \quad (1)$$

where $x_i$denotes the CT-derived morphometric feature vector for case i. The feature vector was defined as:

$$x_i = \left(F_i, d_{GT,i}, d_{LT,i}, NSA_i, L_{calcar,i}, d_{hinge,i}, d_{split,i}, DTI_i, \overline{(HU)_\iota}\right) \quad (2)$$

where the individual parameters are defined in Table 1.

2.2 Eligibility Criteria

Patients aged 18–85 years with a clearly identifiable PHF on non-contrast CT acquired at a slice thickness of 0.625 mm were eligible for inclusion. Cases with pathological fractures, bone tumors, pre-existing implants interfering with CT assessment, or associated injuries precluding reliable morphometric evaluation were excluded.

2.3 Sample Size Estimation

The minimum sample size was estimated using:

$$n = (Z\^2\, p(1-p))/d\^2 \quad (3)$$

where $Z = 1.96$ for a 95% confidence level, $p = 0.757$, based on the proportion reported by Iglesias-Rodríguez et al. [8], and $d = 0.10$. The calculated minimum sample size was 71 cases. A total of 80 eligible PHFs were ultimately included in the analysis.

2.4 CT Processing and Morphometric Measurements

CT datasets were evaluated using RadiAnt DICOM Viewer (version 2023.1) in the bone window. Multiplanar reconstruction (MPR) planes—axial (Π_ax), coronal (Π_cor), and sagittal (Π_sag)—were realigned to the humeral shaft axis before measurements were obtained (Figures 1–2). Linear measurements were recorded in millimeters and angular measurements in degrees.

The assessed morphometric parameters included fragment count (F_i), greater tuberosity displacement (d_GT), lesser tuberosity displacement (d_LT), neck–shaft angle (NSA), intact medial calcar length (L_calcar), medial hinge displacement (d_hinge), and head-split displacement (d_split).

The neck–shaft angle was represented as:

$$NSA_i = \angle(\boldsymbol{u}_(head,i)ⓜ, \boldsymbol{u}_(shaft,i)) \quad (4)$$

where $\boldsymbol{u}_(head,i)$and $\boldsymbol{u}_(shaft,i)$represent the humeral-head and shaft axes, respectively.

The deltoid tuberosity index (DTI) was calculated immediately proximal to the deltoid tuberosity, at the level where the outer cortical borders became approximately parallel, as the ratio of the outer cortical diameter to the inner endosteal diameter:

$$DTI_i = \frac{\mathrm{D_{outer,i}}}{\mathrm{D_{inner,i}}} \quad (5)$$

CT attenuation was assessed in Hounsfield units (HU) using three regions of interest (ROIs). After selecting the corresponding axial CT plane, three circular ROIs were placed within the humeral head at predefined locations, avoiding cortical bone and fracture lines. The final HU value for each case was calculated as the mean of the three measurements:

$$\bar{}HU_i = (HU_(1,i) + HU_(2,i) + HU_(3,i))/3. \quad (6)$$

Algorithmic Representation of the Measurement Workflow

To formalize the morphometric workflow and facilitate its potential future implementation in computer-aided image analysis, the measurement procedure was represented conceptually as follows:

for each case i in D:

```
align_to_shaft_axis(i)

F_i       = count_fragments(i)
d_GT_i    = measure_GT_displacement(i)
d_LT_i    = measure_LT_displacement(i)
NSA_i     = angle(u_head_i, u_shaft_i)
L_calcar_i = measure_intact_calcar(i)
d_hinge_i  = measure_medial_hinge(i)
d_split_i  = measure_head_split(i)
DTI_i     = calculate_DTI(i)
HU_mean_i = mean(HU_ROI1_i, HU_ROI2_i, HU_ROI3_i)

x_i = [F_i, d_GT_i, d_LT_i, NSA_i, L_calcar_i, d_hinge_i, d_split_i, DTI_i, HU_mean_i]
```

This representation describes the analytical workflow used to structure the CT-derived features and does not constitute an independently validated automated algorithm.

All CT measurements were performed by a single investigator according to the predefined measurement protocol. Inter-observer reliability was therefore not assessable, and repeated measurements for intra-observer reliability analysis were not available.

Table 1. Definitions of CT-derived morphometric variables

Variable	Formula / Symbol	Unit	Description
Fragment count	F_i	count	Number of distinct fragments (Figure 3)
GT displacement	d_GT	mm	Greater tuberosity offset (Figure 4)
LT displacement	d_LT	mm	Lesser tuberosity offset (Figure 5)
Neck–shaft angle	NSA = ∠(u_head,u_shaft)	°	Head–shaft axis angle (Figure 6)
Calcar length	L_calcar	mm	Intact medial cortical length (Figure 7)
Medial hinge	d_hinge	mm	Distance of medial cortical hinge displacement (Figure 8)
Head-split gap	d_split	mm	Displacement across articular surface (Figure 9)

Deltoid Index	DTI = D_outer/D_inner	–	CT-derived index of local bone quality (Figure 10)
Bone density	HŪ = (HU1+HU2+HU3)/3	HU	Mean of 3 ROIs (Figure 11–12)

2.5 Fracture Classification and Ischemic-Risk Features

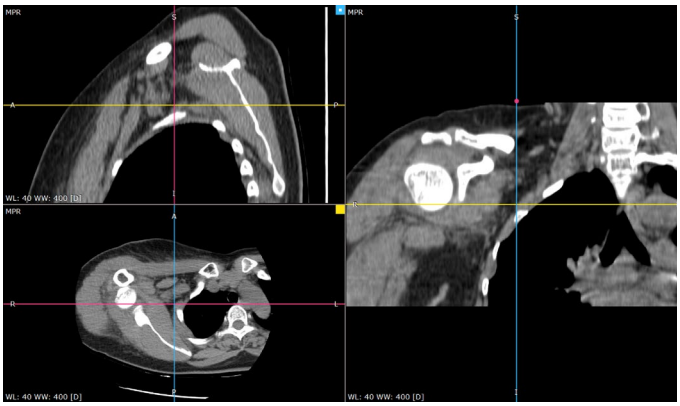


Figure 1. Default three windows in 3D Multiplanar Reconstruction mode

A fracture part was considered displaced according to the Neer criteria when displacement exceeded 10 mm or angulation exceeded 45°.

Morphological features associated with humeral-head ischemic risk were assessed using Hertel-related parameters, including medial calcar extension < 8 mm, medial hinge displacement >2 mm, angular displacement >45°, and the presence of a head-split component.

For the present analysis, cases meeting at least two predefined ischemic-risk features were categorized as having a higher-risk imaging profile.

2.6 Statistical Analysis

Continuous variables were summarized as mean ± standard deviation (SD) or median [interquartile range (IQR)], as appropriate, and categorical variables as frequencies and percentages. Between-group comparisons were performed using the independent-samples t-test or Mann–Whitney U test for continuous variables and the chi-square test or Fisher's exact test for categorical variables, as appropriate. Associations between continuous variables were assessed using Pearson's correlation coefficient. All statistical tests were two-sided, and $p<0.05$ was considered statistically significant. Statistical analyses were performed using IBM SPSS Statistics, version 26.0 (IBM Corp., Armonk, NY, USA).

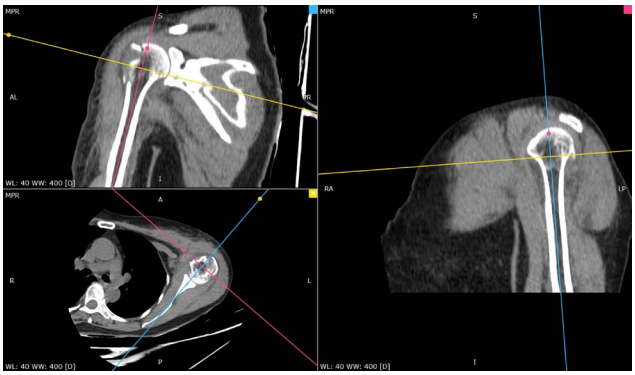


Figure 2. Determination of imaging planes

2.7 Ethical Approval

Approved by the Institutional Ethics Committee (Approval No. 16/GGT-ĐHYD-SĐH). All CT data were anonymized and used solely for research purposes.

3. Results



Figure 3. 3D reconstruction for visualization of fracture fragments

3.1 General Characteristics

From January 2024 to April 2025, a total of 80 proximal humeral fractures (PHFs) meeting inclusion criteria were

analyzed. The mean age was 53.7 ± 16.2 years (range 18–84), with the highest prevalence in the 50–59-year group (31.3%).

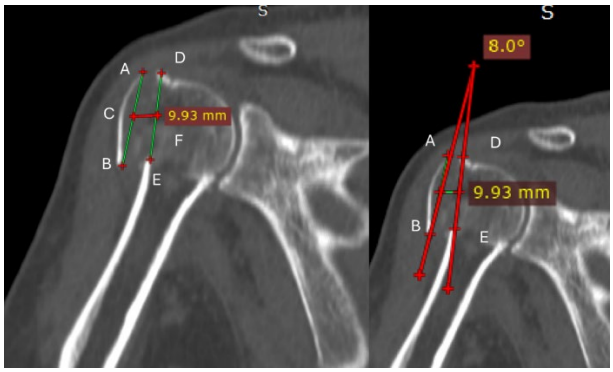


Figure 4. Measurement of displacement and angulation of greater tuberosity fragment

Females accounted for 67.5% of all cases, giving a female-to-male ratio of approximately 2:1. The left side was slightly more affected (52.5%) than the right (47.5%). The demographic characteristics of the study population are summarized in Table 2.

3.2 Fracture Classification

According to the Neer classification, Type II fractures predominated (62.5%), followed by Type III (12.5%) and Type I (10%). Two-part fractures were the most frequent pattern (61.3%), consistent with Neer Type II, while 3-part fractures accounted for 16.3%, and 4-part fractures for 10%.

3.3 Morphological Characteristics by Fragment Type

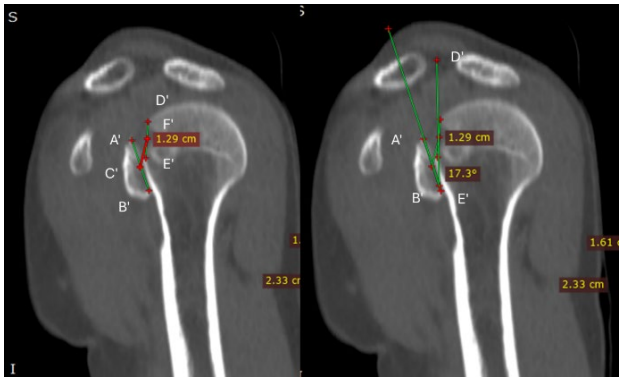


Figure 5. Measurement of displacement and angulation of lesser tuberosity fragment

Greater tuberosity fractures occurred in 67.5% of cases, with a mean displacement 10.43 ± 7.62 mm and angulation 15.67 ± 18.49°. Lesser tuberosity fractures were found in 20% of cases (displacement 12.85 ± 6.29 mm; angulation 29.01 ± 25.36°). Surgical neck fractures (61.3%) showed mean neck–shaft angle 122.2 ± 21.8°, calcar length 6.58 ± 2.47 mm, and medial hinge displacement 1.66 ± 2.17 mm. Detailed morphometric parameters of surgical neck fractures are presented in Table 3. Among surgical neck fractures, 81.6% met ≥2 predefined Hertel-related ischemic-risk features. Anatomical neck fractures (17.5%) had the largest displacement (14.63 ± 9.58 mm) and angulation (37.48 ± 34.93°).

Table 2. Baseline characteristics of the study population (n = 80)

Parameter	n (%) or Mean ± SD	Range
Age (years)	53.7 ± 16.2	18–84
Female	54 (67.5%)	—
Indirect fall	68 (85.0%)	—
Direct trauma	12 (15.0%)	—
Left side	42 (52.5%)	—
Right side	38 (47.5%)	—

Table 3. Morphometric parameters of surgical neck fractures (n = 49)

Parameter	Mean ± SD	Range	n (%) meeting criteria
Neck–shaft angle (°)	122.2 ± 21.8	66.4–164.1	—
Calcar length (mm)	6.58 ± 2.47	1.2–11.4	—
Medial hinge displacement (mm)	1.66 ± 2.17	0.31–15	—
Varus type	—	—	28 (57.1%)
Higher-risk imaging profile (≥2 predefined Hertel-related features)	—	—	40 (81.6%)

3.4. Bone Quality Indicators

The mean Deltoid Tuberosity Index (DTI) was 1.75 ± 0.32. A DTI <1.44, a threshold associated with low bone quality, was observed in 20% of cases. Mean Hounsfield Unit (HU) was 125.1 ± 6.3 HU, with males showing significantly higher HU than females (127.3 ± 6.6 vs. 124.0 ± 5.8 HU, p = 0.028). Bone quality indicators stratified by age and sex are summarized in Table 4.

Table 4. Bone quality indicators by age and sex

Parameter	Mean ± SD	p-value
DTI overall	1.75 ± 0.32	—
DTI <1.44 (low bone quality)	16 (20%)	—
HU – Male	127.3 ± 6.6	0.028*
HU – Female	124.0 ± 5.8	—
HU <50 years	126.6 ± 6.0	0.14
HU ≥70 years	122.4 ± 7.1	—

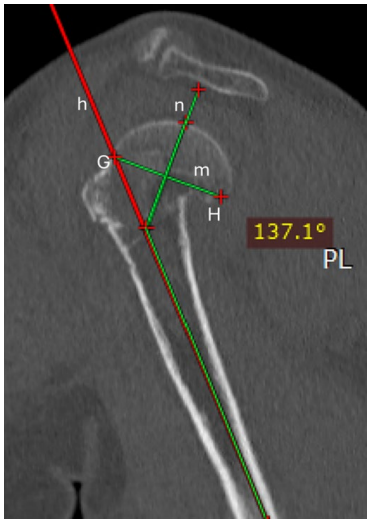


Figure 6. Determination of the neck–shaft angle and fracture pattern

3.5 Association Analyses

Fracture complexity (simple I–II vs. complex III–V) showed no significant association with age (p=0.12), sex (p=0.58), low DTI status (p=0.758), or HU (p=0.91). However, direct trauma was significantly associated with complex fractures (p<0.01). This association between direct trauma and complex fracture configuration highlights the mechanical effect of high-energy impact. The associations between clinical and morphometric factors and fracture complexity are shown in Table 5

.

Table 5. Associations between clinical and morphometric factors and fracture complexity

Variable	Simple (I–II) (n = 58)	Complex (III–V) (n=22)	p-value
Age: <50 / 50–69 / ≥70 years	21 / 29 / 8	3 / 14 / 5	0.12
Sex (Male / Female)	19 / 39	7 / 15	0.58
Mechanism (Direct / Indirect)	1 / 57	11 / 11	<0.01
Low DTI (<1.44), n (%)	11 (19.0%)	5 (22.7%)	0.758†
HU, mean ± SD	125.1 ± 6.1	125.0 ± 6.7	0.91

3.5.1 Summary of Key Findings

- Female predominance (2:1) and indirect trauma were the main patterns.
- Neer Type II and two-part fractures were most common.
- Surgical neck fractures showed a high prevalence of varus deformity, with 81.6% meeting ≥2 predefined Hertel-related ischemic-risk features.
- A DTI <1.44, indicating low bone quality, was found in 20% of cases.
- Bone density (HU) decreased with age but was not statistically significant; only sex differences were significant.
- Fracture complexity was associated with trauma mechanism but not with bone quality.

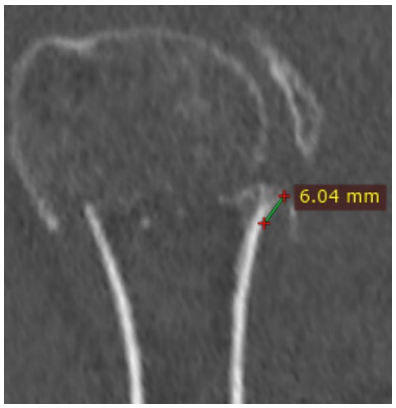


Figure 7. Measurement of the calcar fracture margin

4. Discussion

This study provides a comprehensive CT-based morphometric assessment of proximal humeral fractures (PHFs) in a Vietnamese population. The results highlight important epidemiologic, morphologic, and bone-quality patterns comparable to international data while revealing several distinctive regional characteristics.

4.1 Demographic Characteristics

The present series had a mean patient age of 53.7 ± 16.2 years, notably younger than that reported in Western populations [9], likely reflecting a more active, labor-related trauma profile. The peak incidence occurred in the fifth decade, comparable to the distribution reported by Alzobi et al. [10], whereas Lind et al. [11] observed an elderly-dominant pattern in Scandinavian cohorts.

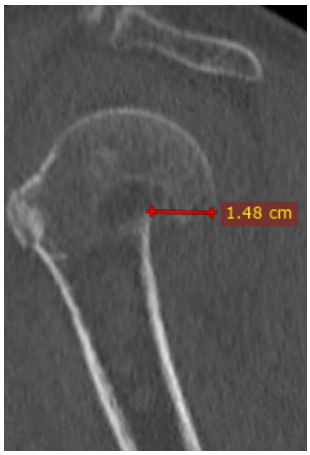


Figure 8. Measurement of medial hinge displacement

A female predominance (67.5%) was observed, in agreement with previous reports attributing higher fracture risk to postmenopausal osteoporosis [11]. Indirect low-energy falls were the main mechanism (85%), matching reports from Iglesias-Rodríguez et al. [8].

4.2 Fracture Pattern and Neer Classification

In our series, Type II fractures were most frequent (62.5%), corresponding to the predominance of two-part fractures (61.3%). Although the study population was relatively young, fracture complexity was significantly associated with trauma mechanism: direct trauma was more frequent among complex fractures than simple fractures (11/22 vs. 1/58, $p < 0.01$). These findings suggest that trauma mechanism, particularly direct trauma, was more closely associated with fracture complexity in our cohort than age alone.



Figure 9. Measurement of displacement and angulation of anatomical neck fracture fragment

Previous studies have reported that CT, particularly with 3D reconstructions, may improve the inter-observer reliability of proximal humeral fracture classification compared with plain radiographs, as reported by Stoddart et al. [12] and Brunner et al. [5]. While CT does not yet uniformly achieve κ >0.8, its enhanced visualization of fragment displacement and treatment-relevant morphology supports its increasing use in proximal humerus fracture assessment.

4.3 Greater Tuberosity Fractures

In our study, greater tuberosity involvement was observed in 67.5% of cases, with a mean displacement of 10.4 mm.

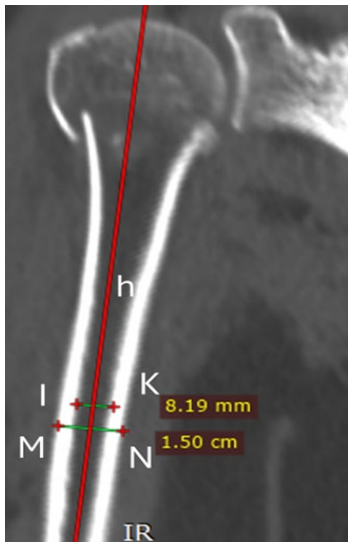


Figure 10. Measurement of the Deltoid Tuberosity Index

Based on the displacement threshold applied, the proportion of cases meeting surgical indication varied markedly—35.2% when using the traditional 10 mm Neer criterion, and 79.6% when adopting a 5 mm cutoff. These

findings are in line with recent literature [13], which has questioned whether the classical 10 mm threshold may underestimate the functional impact of displaced greater tuberosity fractures. Biomechanical models by Bono et al. [14] demonstrated that superior displacement of the greater tuberosity by 5 mm increased the deltoid force required for abduction by 16%, supporting concern regarding even relatively small residual displacement. Consistent with Boksh et al. [15], who reported surgical fixation for displacements > 5 mm and conservative management for < 5 mm, our findings support further evaluation of displacement thresholds in relation to patients' functional demands and activity levels.

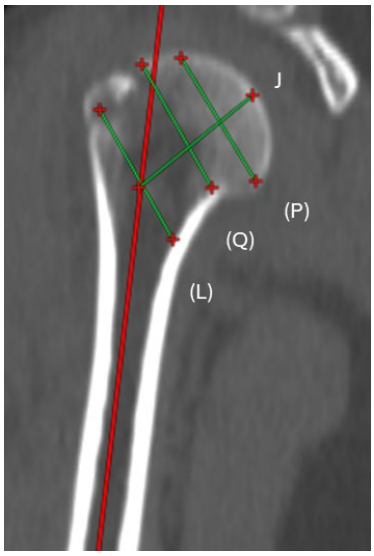


Figure 11. Selection of the corresponding axial slice and definition of three circular regions of interest (ROIs) for Hounsfield unit measurement

4.4 Lesser Tuberosity Fractures

Lesser tuberosity fractures accounted for 20% of cases and were associated with posterior shoulder dislocation in 37.5% of cases in our series. This finding is consistent with the known association between lesser tuberosity fractures and subscapularis injury [16]. Our CT-based analysis showed a mean displacement of 12.9 mm and an angular deviation of 29°, comparable to Ripoll et al. [17], who reported 44% of cases with displacement ≥10 mm on 3D mapping. These results emphasize the necessity of CT evaluation, as 2D radiographs tend to underestimate displacement by approximately 2 mm [17].

4.5 Surgical Neck and Hertel Parameters

Surgical-neck fractures (61.3%) exhibited a mean neck-shaft angle of 122°, with 57% showing varus deformity. Only 30.6% met three of the four predefined Hertel-related ischemic-risk features, whereas 81.6% met ≥2 of these features. Previous studies have associated these morphological features, particularly medial calcar extension <8 mm and medial hinge disruption >2 mm, with impaired humeral-head perfusion and subsequent AVN [18,19]. In the present study, these parameters were used as imaging features associated with humeral-head ischemic risk; however, their association with subsequent AVN was not evaluated. Although Neer displacement thresholds (>10 mm, >45°) remain descriptive, Hertel-related parameters may provide complementary information for fracture characterization and treatment planning.

4.6 Anatomical Neck and Head-Split Fractures

In our series, anatomical-neck fractures were uncommon (17.5%) but demonstrated the greatest displacement (14.6 mm) and angulation (37°). These injuries typically result from high-energy mechanisms and are associated with a high risk of avascular necrosis (AVN) [20]. Cai et al. [20] reported AVN rates up to 43.8% and greater operative complexity for anatomical-neck fractures compared with surgical-neck fractures. No isolated head-split fractures were identified, consistent with their rarity in previous literature.

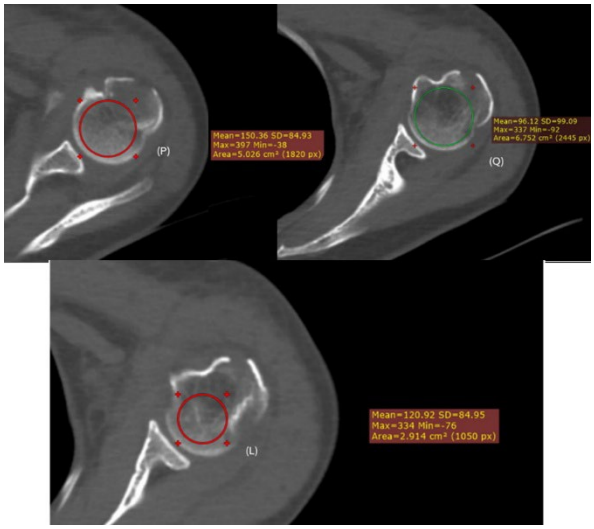


Figure 12. Measurement of Hounsfield unit values in the three corresponding circular regions (P), (Q), and (L)

4.7 Bone-Quality Indicators (DTI and HU)

In our cohort, the mean DTI (1.75 ± 0.32) and HU (125 ± 6.3) indicated generally preserved bone quality. A DTI <1.44, indicating low bone quality, was observed in 20% of patients. The relatively narrow dispersion of HU values (125.1 ± 6.3 HU) may reflect the characteristics of this study population and the standardized ROI-based measurement approach;

however, this finding should be interpreted cautiously given the single-center sample. These values exceed those reported by Kim et al. [21], likely due to our younger population. HU values declined slightly with age and were significantly higher in males ($p = 0.028$), consistent with Liu et al. [22]. No significant association between bone-quality indicators (low DTI status or HU) and fracture complexity was identified, consistent with Liu et al. [22], who found no significant difference in HU values between simple and complex proximal humeral fractures.

4.8 Clinical Implications

Our data indicate that CT-based morphometry provides quantitative evaluation of fragment displacement, calcar integrity, and ischemic-risk features. Integration of quantitative indices such as DTI and HU into CT assessment may provide additional information on local bone quality and may contribute to future risk-stratification approaches. The clinical relevance of alternative displacement thresholds for the greater tuberosity warrants further prospective evaluation in light of existing biomechanical and functional evidence.

Recent studies have demonstrated the potential of deep-learning approaches for the detection and classification of proximal humeral and shoulder fractures on radiographs [23–25]. These findings support the potential value of structured quantitative imaging variables for future computer-aided image-analysis applications. However, no artificial intelligence or machine-learning model was developed or validated in the present study.

4.9 Limitations

This was a single-center study with a limited sample size ($n = 80$), lacking postoperative outcomes and formal intra- and inter-observer reliability assessment. HU and DTI were measured on fractured humeri rather than the contralateral side, possibly affecting accuracy. Future multicenter studies combining CT morphometry with clinical outcomes and DEXA-validated bone density are warranted.

5. Conclusion

This study proposed a quantitative and algorithmic framework for the morphometric evaluation of proximal humeral fractures (PHFs) based on computed tomography (CT). The structured quantitative variables and conceptual algorithmic workflow may provide a basis for future computer-aided image-analysis applications. However, no automated classification, machine-learning model, or clinical decision-support system was developed or validated in the present study. Future studies should evaluate observer reliability, correlate CT-derived parameters with clinical outcomes, and prospectively validate their potential integration into automated image-analysis systems.

Acknowledgement

The authors express their sincere gratitude to the Department of Radiology of Hospital for Traumatology and Orthopaedics in Ho Chi Minh City and the Department of Orthopaedics and Rehabilitation, University of Medicine and Pharmacy at Ho Chi Minh City.

References

[1] Court-Brown CM, Caesar B. Epidemiology of adult fractures: A review. Injury. 2006;37(8):691–697.
[2] Launonen AP, Lepola V, Saranko A, Flinkkilä T, Laitinen M, Mattila VM. Epidemiology of proximal humerus fractures. Arch Osteoporos. 2015;10:209.
[3] Court-Brown CM, Duckworth AD, Clement ND, McQueen MM. Fractures in older adults. A view of the future? Injury. 2018;49(12):2161-2166.
[4] Sukthankar AV, Leonello DT, Hertel RW, Ding GS, Sandow MJ. A comprehensive classification of proximal humeral fractures: HGLS system. J Shoulder Elbow Surg. 2013;22(7):e1-6.
[5] Brunner A, Honigmann P, Treumann T, Babst R. The impact of stereo-visualisation of three-dimensional CT datasets on the inter- and intraobserver reliability of the AO/OTA and Neer classifications in the assessment of fractures of the proximal humerus. J Bone Joint Surg Br. 2009;91(6):766-771.
[6] Berkes MB, Dines JS, Little MTM, Garner MR, Shifflett GD, Lazaro LE, et al. The impact of three-dimensional CT imaging on intraobserver and interobserver reliability of proximal humeral fracture classifications and treatment recommendations. J Bone Joint Surg Am. 2014;96(15):1281–1286.
[7] Bahrs C, Laux CJ, Josten C, Wissing F. Assessment of proximal humeral fractures: Does CT (2D/3D) provide additional benefit compared to conventional radiographs? BMC Musculoskelet Disord. 2010;11:233.
[8] Iglesias-Rodríguez S, Domínguez-Prado DM, García-Reza A, Fernández-Fernández D, Pérez-Alfonso E, García-Piñeiro J, et al. Epidemiology of proximal humerus fractures. J Orthop Surg Res. 2021;16(1):402.
[9] Polykandriotis E, Zschiegner A, Horch RE, Schürmann M. Bone allograft and locking plate for severe proximal humeral fractures: early and late outcomes. Med Sci Monit. 2021;27:e928982.
[10] Alzobi OZ, Salman LA, Derbas J, Abudalou A, Hantouly AT, Ahmed G. Epidemiology of proximal humerus fractures in Qatar. Eur J Orthop Surg Traumatol. 2023;33(7):3119-3124.
[11] Lind T, Krøner K, Jensen J. The epidemiology of fractures of the proximal humerus. Arch Orthop Trauma Surg. 1989;108(5):285–287.
[12] Stoddart M, Pearce O, Smith J, McCann P, Sheridan B, Al-Hourani K. Proximal humerus fractures: reliability of Neer versus AO classification on plain radiographs and computed tomography. Cureus. 2020;12(6):e8520.
[13] Janssen SJ, Jayakumar P, Ter Meulen DP, van Deurzen DFP, Ring D. Quantitative 3-dimensional computerized tomography modeling of isolated greater tuberosity fractures with and without shoulder dislocation. Arch Bone Jt Surg. 2019;7(1):24-32.
[14] Bono CM, Renard R, Levine RG, Levy AS. Effect of displacement of fractures of the greater tuberosity on the mechanics of the shoulder. J Bone Joint Surg Br. 2001;83(7):1056-62.

[15] Boksh K, Srinivasan A, Perianayagam G, Singh H, Modi A. Morphological characteristics and management of greater tuberosity fractures associated with anterior glenohumeral joint dislocation: a single centre 10-year retrospective review. J Orthop. 2022;34:1-7.
[16] Spek RWA, Schoolmeesters BJA, den Haan C, Jaarsma RL, Doornberg JN, van den Bekerom MPJ. What are the patient-reported outcomes, functional limitations, and complications after lesser tuberosity fractures? A systematic review of 172 patients. JSES Int. 2021;5(4):754-764.
[17] Ripoll T, Chelli M, Johnston T, Chaoui J, Gauci MO, Vasseur H, et al. Three-dimensional measurement of proximal humerus fractures displacement: a computerized analysis. J Clin Med. 2023;12(12):4085.
[18] Fazzari F, Canton G, Giraldi G, Falcioni N, Clocchiatti S, Rasio N, et al. Avascular necrosis of humeral head after proximal humerus fracture: comparison between classification systems in predicting necrosis risk. Acta Biomed. 2023;94(S2):e2023089.
[19] Campochiaro G, Rebuzzi M, Baudi P, Catani F. Complex proximal humerus fractures: Hertel's criteria reliability to predict head necrosis. Musculoskelet Surg. 2015;99 Suppl 1:S9-15.
[20] Cai P, Yang Y, Xu Z, Wang Z, Zhou X, Yang T. Anatomic locking plates for complex proximal humeral fractures: anatomic neck fractures versus surgical neck fractures. J Shoulder Elbow Surg. 2019;28(3):476-482.
[21] Kim DM, Park D, Kim H, Lee ES, Shin MJ, Jeon IH, et al. Risk factors for severe proximal humerus fracture and correlation between deltoid tuberosity index and bone mineral density. Geriatr Orthop Surg Rehabil. 2020;11:2151459320938571.
[22] Liu G, Li L, Yang C, Wei L, Li T, Zhu L, et al. Hounsfield units predicts the occurrence but not the patterns of proximal humerus fracture in the elderly patients. BMC Musculoskelet Disord. 2023;24(1):342.
[23] Chung SW, Han SS, Lee JW, Oh KS, Kim NR, Yoon JP, et al. Automated detection and classification of the proximal humerus fracture by using deep learning algorithm. Acta Orthop. 2018;89(4):468-473.
[24] Magnéli M, Ling P, Gislén J, Fagrell J, Demir Y, Arverud ED, et al. Deep learning classification of shoulder fractures on plain radiographs of the humerus, scapula and clavicle. PLoS One. 2023;18(8):e0289808.
[25] Sperling JW Jr, Yang L, Girod MM, Saniei S, Kaji ES, Grove AF, et al. A deep learning algorithm to detect proximal humerus fractures on radiographs. JSES Rev Rep Tech. 2025;5(4):635-640.